Journal of Sound and Vibration 330 (2011) 182–193

Contents lists available at ScienceDirect

Journal of Sound and Vibration

journal homepage: www.elsevier.com/locate/jsvi

# Semi-active particle-based damping systems controlled by magnetic fields

Binoy M. Shah, Jeremy J. Nudell, Kevin R. Kao, Leon M. Keer*, Q. Jane Wang, Kun Zhou

*Department of Mechanical Engineering, Northwestern University, 2145 Sheridan Road, Evanston, IL 60208-3109, USA*

ARTICLE INFO

*Article history:*
Received 5 September 2009
Received in revised form
3 June 2010
Accepted 3 August 2010
Handling Editor: M.P. Cartmell
Available online 18 September 2010

ABSTRACT

This paper reports the design of a semi-active particle-based damping system in which a dry magnetic particle bed is used to dissipate the energy of a vibrating piston. The system is magnetized by a magnetic field generated by an electromagnetic coil. Hysteresis-free, ferromagnetic materials are selected for both the piston and particles. The damping efficiency increases as the magnetization of the piston and particles increases up to saturation. Semi-active control is achieved by varying the electric current supplied to the coil, which changes the magnetization and allows for real-time tunability of the damping rate. During the process of magnetization and demagnetization, the damping is reversible and temperature-independent over a wide temperature range. This system can be useful in aerospace, automobile and structural engineering applications, particularly in harsh environments.



## 1. Introduction

Vibration damping systems for structural control are often required to operate under variable load conditions, over wide frequency ranges and in extreme temperature environments. Passive, active and semi-active vibration control methods are used to provide external damping for aerospace, automotive and civil engineering applications [1–5].

Passive systems use viscous fluids, visco-elastic materials or tuned masses as dampers to dissipate energy without the use of actuators and external power supply. However, such systems are most effective only in a narrow frequency range. Moreover, their performance is hampered by a detuning effect because of which, over time, they are unable to provide the level of vibration suppression originally designed for. Detuning can occur either as a result of deterioration of the damper or due to changes in the excitation or natural frequency of the vibrating structure. Passive damping systems, although widely used, have applications limited by their inability to adapt to varying usage patterns, loading conditions and frequency ranges [1]. Active damping systems can produce desired response characteristics for a variety of disturbances by using actuators to provide an active force to the vibrating structure. However, active systems are often limited in their use because their actuators require a large external source of power [6].

A semi-active damping system addresses the limitations of the passive and the active system by integrating tunable control into a passive device [3], by replacing force actuators with continually adjustable control elements which are capable of modifying a damper's energy dissipation rate in response to excitation conditions. Therefore, semi-active devices are also referred to as variable-rate or adaptive-passive dampers. This damping method is attractive because it requires a significantly lower amount of external power supply, as compared to the active system. Since semi-active

* Corresponding author. Tel.: +1 847 491 4046.
*E-mail address:* l-keer@northwestern.edu (L.M. Keer).

0022-460X/$ - see front matter © 2010 Elsevier Ltd. All rights reserved.
doi:10.1016/j.jsv.2010.08.009

devices do not employ force actuators, they do not produce excessive mechanical energy which can destabilize a structure. Furthermore, a semi-active system is considered fail-safe because in the event of a power-failure it can still function as a passive damping system. Examples of semi-active systems include controllable fluid dampers, variable orifice fluid dampers, controllable friction devices, variable-stiffness devices and smart tuned mass dampers.

Magneto-rheological (MR) fluid-based dampers are the most popular semi-active devices [7–10]. A MR fluid is composed of microsized, magnetically polarizable particles dispersed in a carrier medium such as mineral or silicone oil. In a magnetic field, MR fluid has the ability to reversibly transform in milliseconds from free-flowing to linear viscous and then to semi-solid with controllable yield strength, while requiring a small power supply of less than 50 W. However, this damping medium has several disadvantages. For example, its operating temperature range is limited from $-40^\circ$ to $150^\circ$ C [7]; it can leak out of a device and damage other components; and its particle dispersion can settle out when subjected to high gravitational forces [11]. Since the medium is a fluid, it is also unsuitable for use in a vacuum environment.

In this research, a new concept for a semi-active thrust damping system is proposed, in which a piston oscillates vertically in a dry magnetic particle bed. The particles serve as the damping medium, and the particle–particle and particle–piston interactions serve as the damping mechanisms. The strength of the interactions is controlled by an external magnetic field to provide tunable damping. This system benefits from the dual solid- and liquid-like nature of the particle medium. The solid-like nature allows the particles to have a significantly wider operating temperature range, avoid fluid-like leakage issues and operate in vacuum environments. The liquid-like nature enables the particles to flow and re-organize, thereby preventing settling or fatigue in the system. A particle medium is also chemically and physically stable, low in cost, commercially available and easy to use.

This paper describes the design of a particle-based semi-active damping system and the experimental analysis of its performance. The key components of the design are discussed in Section 2, an experimental system built to characterize the damping is presented in Section 3, and the experimental results revealing the performance of the damping system are given in Section 4.

## 2. Design of the damping system

The designed damping system (Fig. 1) contains three essential components: (1) an oscillating thrust piston to transfer energy from a vibrating mass to the damping medium, (2) magnetic particles to dissipate energy and serve as tunable damping medium, and (3) an electromagnet to generate a magnetic field of desired strength. The thrust piston is a cylindrical metal rod with flat ends. It is made from either steel (12L14 carbon steel) to produce a magnetic piston or aluminum to produce a non-magnetic one. The properties of the magnetic particles and the electromagnet are presented in detail hereafter.

### 2.1. Properties of the magnetic particles

The damping medium must be selected based on its magnetic, thermal and mechanical properties. Particles made of AISI 52100 chrome steel (Fox Industries) were selected because of their large magnetic susceptibility, resistance to high temperatures, and high strength to endure repeated loadings. These particles (see Fig. 2a) are spherical with diameter $d=1.2\pm0.1$ mm, density $\rho=7800$ kg/m$^3$, melting point temperature of $1500^\circ$ C and Young's modulus of 193 GPa.

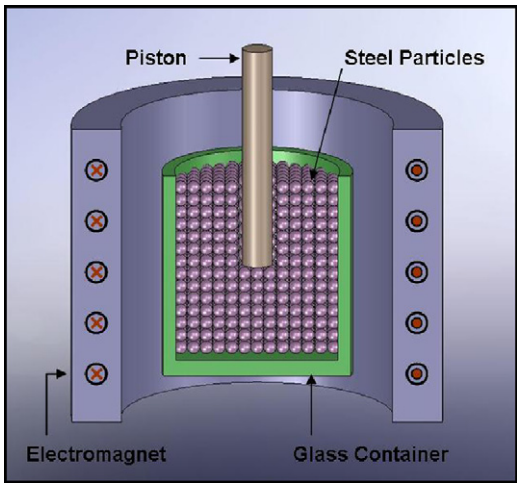


**Fig. 1.** Components in the design of a particle-based semi-active thrust damping system.

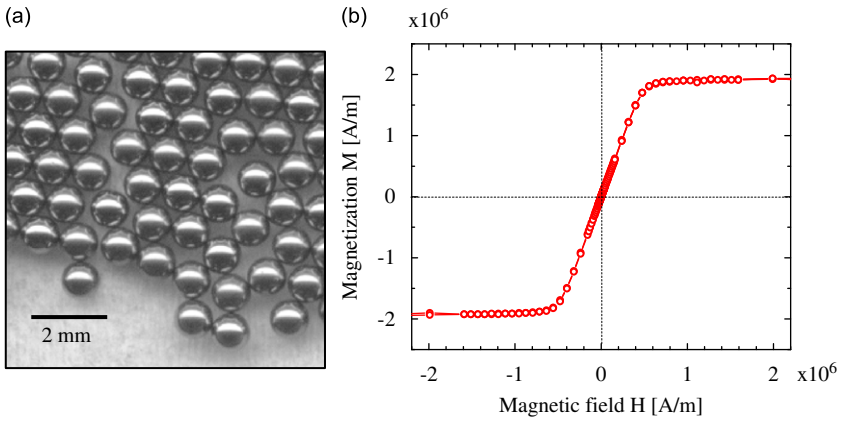


**Fig. 2.** (a) Image of 1.2 mm chrome steel particles and (b) their magnetic response to an applied field.

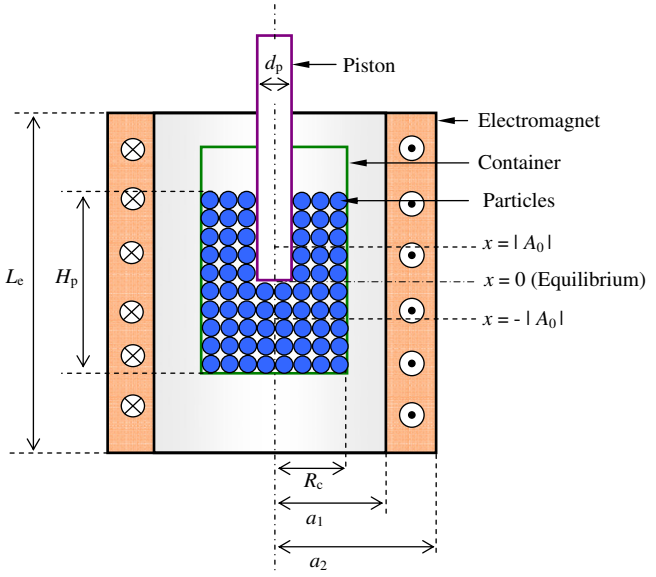


**Fig. 3.** Configuration of the piston, the particle bed, the container and the electromagnet as arranged in the experimental setup.

The magnetization $M$ induced by an applied magnetic field $H$ at room temperature ($T$=24 °C) is experimentally measured using a sensitive magnetometer. Fig. 2b shows that, in its $M(H)$ magnetic hysteresis curve, a chrome steel particle does not exhibit any hysteretic behavior and therefore its magnetization is completely reversible. As a result, the particle does not retain any residual magnetic moment once the field is removed. The onset of magnetization occurs immediately once $|H| > 0$, suggesting that the particles can respond instantly to the field. For $|H| < 0.47 \times 10^6$ A/m, $M$ is linearly dependent on $H$. The slope of the linear region represents the initial susceptibility of the magnetic mass $\chi_{in}=M/H=3.6$ and refers to the degree of magnetization of a material in response to the field. For $|H| \geq 0.47 \times 10^6$ A/m, $M$ saturates at $1.94 \times 10^6$ A/m and $\chi_{in}=0$, which means the particles cannot be further magnetized by increasing $|H|$.

Particles act like dipoles when magnetized, and the magnetic force between two particles is caused by the dipole–dipole interaction. If $z$ is the separation distance between the surfaces of two particles, the dipolar forces are inversely proportional to $z^3$ and are thus of long-range nature. The force is dependent on the shape rather than the size of the particle.

### 2.2. Properties of the electromagnet

The arrangement of the piston, the particle bed, and the electromagnet is shown in Fig. 3 and their dimensions are given in Table 1. The particle-filled container is surrounded by an electromagnetic coil, which can generate a magnetic field of magnitude $H$ based on the direct current $I$ supplied to it. The generated field can magnetize both the piston and the

**Table 1**
Dimensions of the experimental configuration.

| Dimension | Symbol | Value (mm) |
|---|---|---|
| Diameter of the particle | $d$ | 1.2 |
| Diameter of the piston | $D_p$ | 9.5 |
| Inner radius of the container | $R_c$ | 27.3 |
| Height of the particle bed | $H_p$ | 40.0 |
| Immersion depth of the piston | $L$ | 20.0 |
| Initial vibration amplitude | $A_0$ | −10.0 |
| Height of the electromagnet | $L_e$ | 90.0 |
| Inner radius of the electromagnet | $a_1$ | 90.0 |
| Outer radius of the electromagnet | $a_2$ | 122.0 |

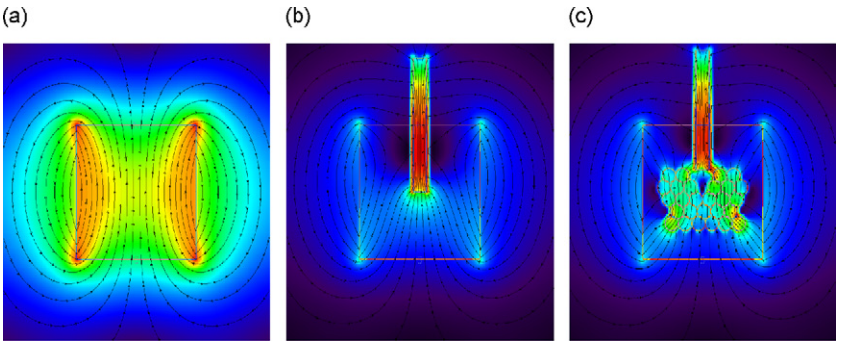


**Fig. 4.** Simulation results for the magnetic field and flux density inside a solenoid which contains (a) free space, (b) magnetic piston, or (c) magnetic particles with a magnetic piston.

particles. Varying the magnitude of $H$ can change the strength of the magnetic inter-particle interactions and thus provide tunable control.

The coil used in the experiments has the length $L_e$=90 mm, the inner winding radius $a_1$=90 mm, the outer winding radius $a_2$=122 mm, the number of turns $N$=3400, and a resistance of 6.25 Ω. The magnetic field $H_0$ at the center of a thick coil of finite length is given as [12]

$$H_0 = \frac{NI}{a_1}\frac{1}{2\beta_2(\beta_1-1)}G(\beta_1,\beta_2) \tag{1}$$

where $\beta_1=a_2/a_1$, $\beta_2=L_e/2a_1$, and $G(\beta_1,\beta_2)$ is a geometry dependent field factor given by

$$G(\beta_1,\beta_2) = \frac{4\pi\beta_2}{10}\left(\sinh^{-1}\frac{\beta_1}{\beta_2}-\sinh^{-1}\frac{1}{\beta_2}\right) \tag{2}$$

When $I$=0.5 A is supplied, a magnetic field $H_0=7.4\times10^3$ A/m is generated at the center of the coil which produces a magnetic induction, also known as flux density $B=\mu H$ in the medium of permeability $\mu$ present within the field. In the case where the coil contains only free space, the permeability $\mu=\mu_0=4\pi\times10^{-7}$ H/m and relative permeability $\mu_r=\mu/\mu_0=1$. Therefore, a magnetic induction $B_0$=9.32 mT is produced at the center of the coil. The field outside the coil is generally weak and not suitable for magnetizing materials.

### 2.3. Simulation of magnetic field and flux density

Simulation and analysis of magnetic field and flux density in a configuration similar to that of the experimental setup is performed using an electromagnetic modeling software ViziMag. An electromagnet is modeled as a two-dimensional, thin and straight solenoid with the values for its height, inner radius and number of turns matching that of the actual solenoid used in the experiment. The core of the solenoid contains free space. The magnetic thrust piston is modeled as a rectangular magnetic region having a width of 10 mm. The steel piston is set with $\mu_r$=500 [13]. Circular magnetic regions are used to model 27 individual magnetic particles, each with $\mu_r$=500, and diameter $d$=10 mm, which is 10 times larger than the size used in experiments to aid in visualization of the field. The glass container that holds the particle bed does not affect the magnetic field and therefore it is not modeled in the simulation.

The simulation results are presented in Fig. 4 in which the lines represent the magnetic field $H$ and the contours represent the flux density $B$. Fig. 4a shows the field inside a solenoid containing free space. At the center of the solenoid, the

field lines are the most uniform and the flux density is $B_0$=10.9 mT, which is approximately the same as that for analytical calculation validating the simulation model. The maximum flux density is $B_{max}$=20.4 mT, and the minimum flux density is $B_{min}$=1.56 mT. When a steel piston is inserted into the solenoid, the piston becomes magnetized and concentrates the magnetic flux at its tip making it a highly attractive region, as seen in Fig. 4b. The flux density at the tip located at the center of the solenoid is $B_0$=26.2 mT which is twice the value obtained in the absence of the piston. The piston also magnifies the flux density, resulting in $B_{max}$=68.5 mT and $B_{min}$=1.48 mT. Steel particles also become magnetized when introduced inside the solenoid, as shown in Fig. 4c. They become dipoles, aligning themselves along the flux path, attracting one another and aggregating around other magnetic regions such as the tip of the piston. The presence of the particles magnifies the flux density even further to $B_{max}$=117.0 mT and $B_{min}$=1.17 mT. Figs. 4b and c also show that magnetic flux is inhomogeneously distributed since the flux paths are confined primarily to magnetically permeable regions.

## 3. Description of the experimental system and procedure

An experimental system is built to test the feasibility and demonstrate the efficiency of the proposed design.

### 3.1. Experimental system

The setup is designed as a single degree of freedom, free vibrating, mass–spring–damper system (Fig. 5). The piston is attached to the bottom of a shuttle, which slides up and down a linear air bearing. The bearing guides the motion of the piston in the vertical direction with negligible internal friction. The vibrating mass $m$ is the sum of the masses of the piston, the shuttle and the sensors (i.e. accelerometer and load cell). For a steel piston, the mass is measured as $m$=0.635 kg; for an aluminum piston, $m$=0.573 kg. Four extension springs are attached to the mass and connected in parallel. The springs provide stiffness and elastic energy to the mass and enable the free vibrating motion of the piston. A particle bed filled with magnetically susceptible metal particles held in a glass container serves as the damping medium. Damping is produced as the piston oscillates in the particle bed. In the absence of the particles, the system is called undamped. However, the undamped system still has inherent damping caused by loss factors such as internal friction and air resistance.

Damping is characterized by measuring the displacements, forces and accelerations of the piston. The displacements are recorded by a laser sensor (Micro-epsilon) with 1 μm resolution and 2500 Hz frequency, accelerations measured by a $\pm 5$ g MEMS accelerometer (Analog Devices), and forces recorded by a load cell (Honeywell-Sensotec) with a maximum capacity of 111.2 N (25 lb) in tension and compression and a full scale resolution of 0.1%.

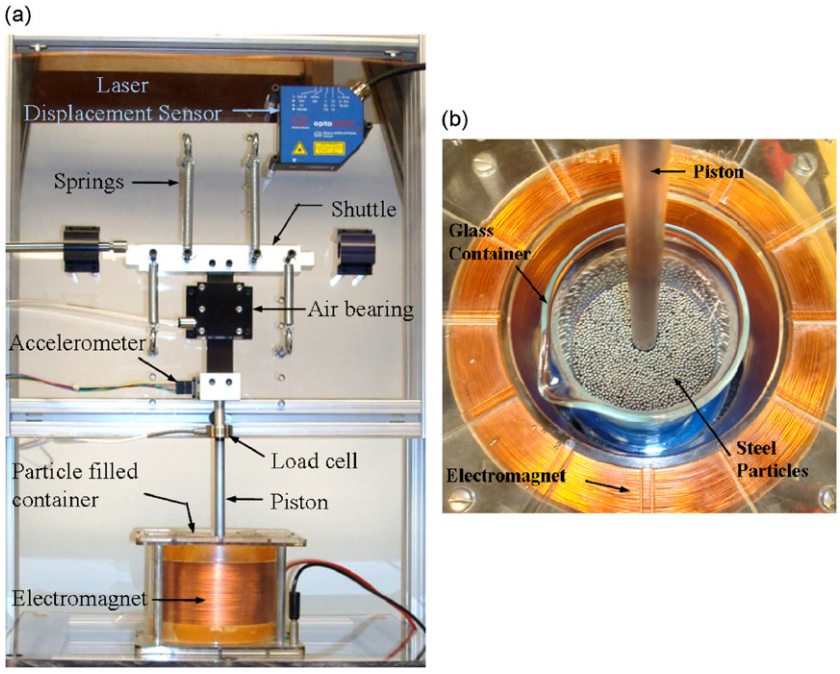


**Fig. 5.** (a) Experimental setup and (b) a close-up of the particle-filled container inside the electromagnet.

### 3.2. Experimental procedure

The experimental procedure consists of six steps: (1) preparing the particle bed, (2) placing the bed inside an electromagnet, (3) immersing a piston in the particle bed, (4) generating the desired amount of magnetic field, (5) providing the piston with an initial displacement, and (6) recording the vibration response of the piston.

The particle bed was prepared by pouring the particles into a cylindrical glass container up to a column height of $H_p$ (see Fig. 3). The particles were then stirred to ensure uniform random packing. The top of the container was left open and the top of the particle bed was considered as a free surface, as no constraints were applied there. The particle-filled container was then placed inside an electromagnet such that the vertical center of the bed matched that of the electromagnetic. Thereafter, the piston was immersed into the bed up to a depth $L=H_p/2$ which is the distance from the top of the bed to the bottom of the piston. The piston, the container and the electromagnet were all horizontally positioned to be concentric. Such an arrangement placed the tip of piston during its equilibrium position at the center of the electromagnet, where the magnetic field was the most uniform. Current was supplied to electromagnet and a magnetic field produced. The piston was given an initial downward displacement $A_0$ to provide initial potential energy to the system and then released. The ambient temperature during the experiments was $25 \pm 3^{\circ}$ C and the relative humidity was $24 \pm 5\%$.

## 4. Experimental results

The performance of the proposed design is evaluated in terms of its damping effectiveness, range of tunability, demagnetization response and sensitivity to temperature.

### 4.1. Damping performance

The feasibility of obtaining semi-active control is examined by comparing the displacement, force and energy decay trends obtained from three experiments. Experiment 1 measures the undamped response in which particles are not present. Experiments 2 and 3 measure the damping produced by un-magnetized and magnetized particles, respectively.

Fig. 6 plots the displacements $x(t)$ and damping force $F_d(t)$ for the three experiments. In Experiment 1, the undamped system shows negligible displacement decay and damping force, which is expected. It is thus assured that the inherent damping produced by the experimental setup does not contribute background noise to the damping results. The

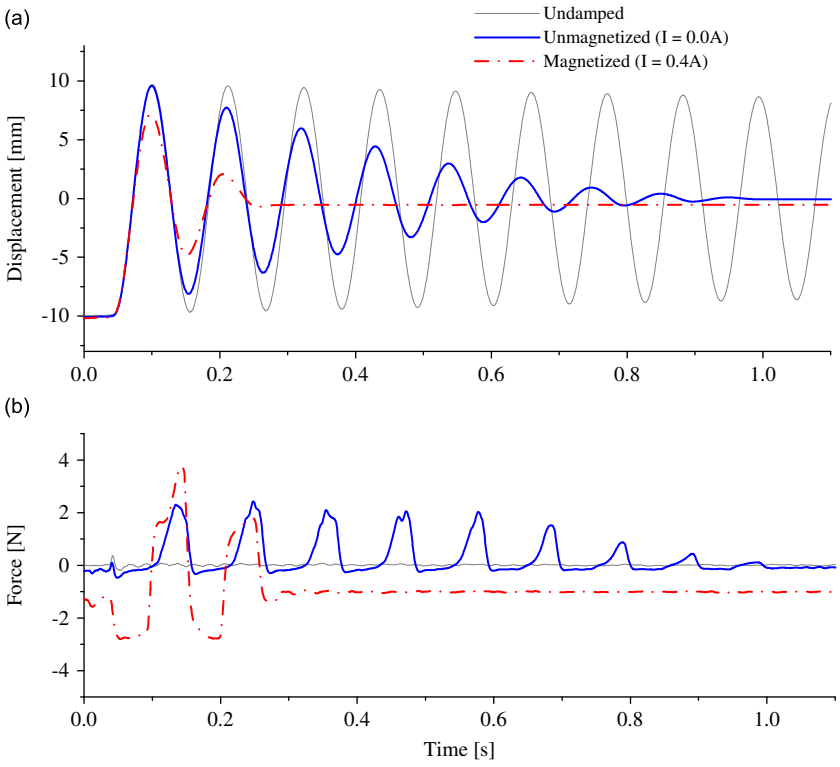


**Fig. 6.** (a) Displacement $x(t)$ and (b) damping force $F_d(t)$ for a magnetized, an un-magnetized and an undamped system.

undamped frequency is measured as $f_n$=8.93 Hz and the stiffness is calculated to be $k_n$=1998 N/m based on the relationship:$f=\sqrt{k/m}/(2\pi)$.

In Experiment 2, the performance of a passively damped system is characterized by employing particles as the damping medium without applying any magnetic field ($I$=0.0 A). It is observed that the displacement decays rapidly and all the vibrations are damped in less than 1.0 s. Thus, particles are effective as a passive damping medium. The damping force is large during each downstroke and nearly zero during each upstroke, suggesting that the damping process is uni-directional and occurs only during half of a cycle. The maximum force value is 2.3 N. The damped frequency is $f_d$=9.33 Hz and the stiffness is $k_d$=2184 N/m, assuming that the mass is constant. The damped stiffness is greater than the undamped one as a consequence of the stiffness contribution of the particle bed. The values of $k_n$ and $k_d$ are used to calculate the energy in the system.

In Experiment 3, a magnetic field generated by current $I$=0.4 A is introduced to magnetize the particles and the piston. This setup represents the semi-active system. Fig. 6 shows that once the magnetic field is turned on, the displacement decay rate increases significantly from that of the passive system. This evidence suggests that damping rate in a particle-based thrust damping system can be controlled by a magnetic field. The damping rate in the magnetized system is much greater than in the un-magnetized system because the damping is bi-directional, i.e. $|F_d(t)|>0$ throughout each vibration cycle, and the maximum damping force is 3.8 N which is nearly twice that as in the un-magnetized system (Fig. 6).

The hysteresis loops for force–displacement $F_d(x)$ and force–velocity $F_d(\dot{x})$relationships are presented in Fig. 7. The area covered by each loop of $F_d(x)$ represents the energy dissipated per cycle. The damping force is highly nonlinear and its magnitude varies with piston depth and velocity. For the un-magnetized system, the force increases linearly during the downstroke, while the force is constant with a value close to zero during the upstroke. In the magnetized system, the force remains constant at negative velocity and it becomes nonlinear at positive velocity. A constant force represents constant friction, while a linearly increasing force represents an increase in the magnitude of friction. The force increases with depth because of an increase in granular pressure. The force during an upstroke is negligible due to the lack of frictional drag on the piston.

The damping results are further analyzed by calculating the energy of the system. Based on the work–energy principle, the total energy is the sum of potential energy and kinetic energy. If $t=t_i^{\alpha}(i\geq 1)$ is denoted as the discrete moments when $x(t)$ reaches its valley value ($\alpha$=1) and peak value ($\alpha$=2) during the $i$th cycle, the velocity is zero at such moments as so is the kinetic energy. As a result, the total energy at the beginning of each cycle is determined only by the potential energy, i.e.

$$E(t_i^{\alpha})=\tfrac{1}{2}kx^2(t_i^{\alpha}) \tag{3}$$

and the energy lost within one cycle is obtained by

$$W(t_i^{\alpha})=E(t_i^{\alpha})-E(t_{i+1}^{\alpha}) \tag{4}$$

The damping capacity $\Omega(t_i^{\alpha})=W(t_i^{\alpha})/E(t_i^{\alpha})$ is the ratio of the energy lost per cycle to the initial system energy. Similarly, the specific damping capacity $\Psi(t_i^{\alpha})=W(t_i^{\alpha})/E(t_i^{\alpha})$ is ratio of the energy lost per cycle to the energy at the start of the cycle. The characteristics for $\Omega(t_i^1)$ and $\Psi(t_i^1)$ are shown in Figs. 8 (a) and (b), respectively. Data for $I$=0.2 A is presented to elucidate the trends.

In Fig. 8a, each data point represents the work done per cycle. The work done in the first cycle increases from 34% to 77% as $I$ increases from 0.0 to 0.4 A, which is a 10% increase for every 0.1 A of additional current. In Fig. 8b, the damping efficiency $\Psi(t_i^{\alpha})$ in one cycle is shown as a function of the non-dimensional acceleration $\Gamma(t_i^{\alpha})=(2\pi f_d)^2x(t_i^1)/g$ where $x(t_i^1)$ is the amplitude at the beginning of the cycle and $g$ the acceleration of gravity. When $\Gamma$=1, the acceleration of the piston is equal to the acceleration due to gravity. Fig. 8b shows that thrust damping with a magnetized system is efficient for a range of accelerations including $\Gamma<1$. In particular, as $I$ increases, $\Psi$ increases at all acceleration levels. This suggests that a

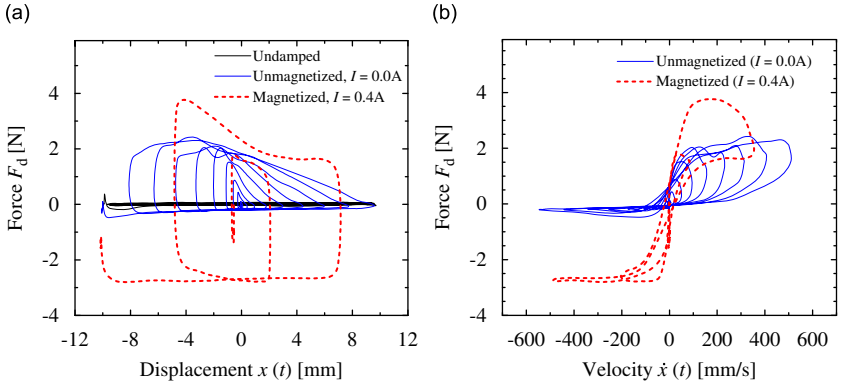


**Fig. 7.** Hysteresis loops for (a) force–displacement relationship $F_d(x)$ and (b) force–velocity relationship $F_d(\dot{x})$.

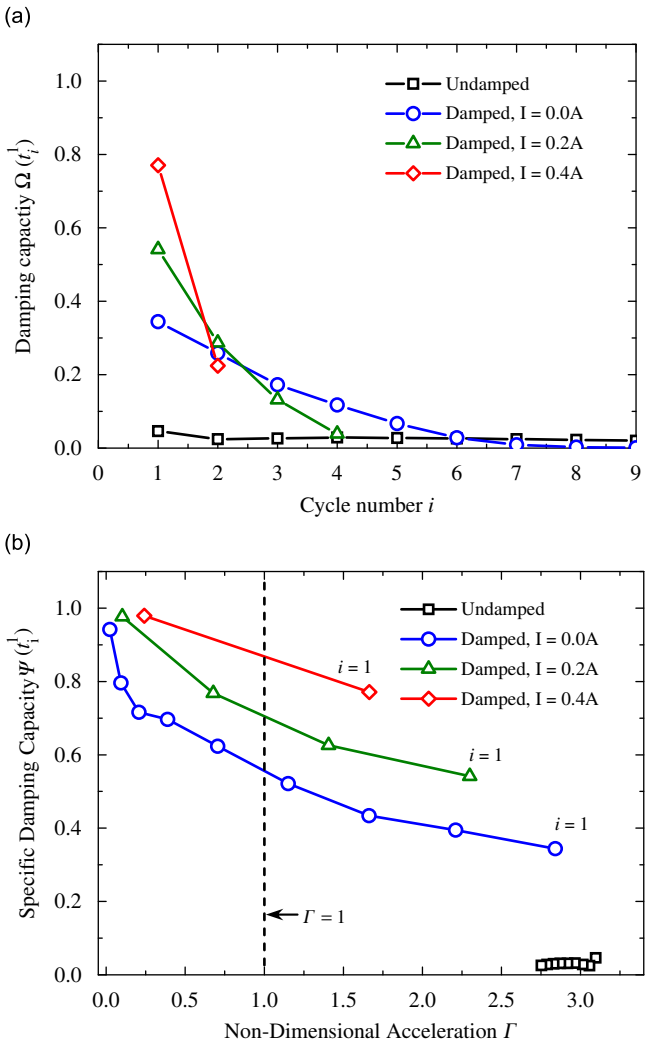


**Fig. 8.** Energy trends shown as (a) damping capacity and (b) specific damping capacity as a function of the non-dimensional acceleration.

semi-active system can improve the damping efficiency for each cycle regardless of its acceleration level. This capability allows the damper to be effective for applications which need to withstand vibrations with frequency and excitation levels over a wide range. In contrast, such capability does not exist for a typical vertical cavity-filled particle damper for which $\Psi=0$ when $\Gamma<1$ [15]. Furthermore, the damping efficiency of a cavity-filled damper would decrease if its particles were magnetized since that would decrease the number of free particles available for collision which is its primary damping mechanism.

### 4.2. Damping with a non-magnetic piston

Different materials react in different ways when affected by a magnetic field. The magnetic properties of materials selected for the piston and the particles should be carefully considered as they can affect the damping capabilities of the semi-active system. A comparison experiment was also done by replacing the steel piston, which is strongly magnetic, with aluminum one which is essentially non-magnetic.

For the un-magnetized system ($I$=0.0 A), it is observed that both magnetic (steel) and non-magnetic (aluminum) piston produce the same amount of damping. However, as $I$ increases, damping with a non-magnetic piston decreases, which is opposite to the trend obtained with a magnetic piston. Fig. 9a shows that the displacement decay with a non-magnetic piston for a highly magnetized system ($I$=0.4 A) is the same as that of the undamped system, suggesting that the negligible damping is produced. This behavior can be explained by considering the relative strengths of interactions between the various magnetic regions, i.e. particle–particle and particle–piston adhesion. Table 2 shows four states which represent different combinations of the particle–particle and particle–piston adhesion, and their resulting damping capacities.

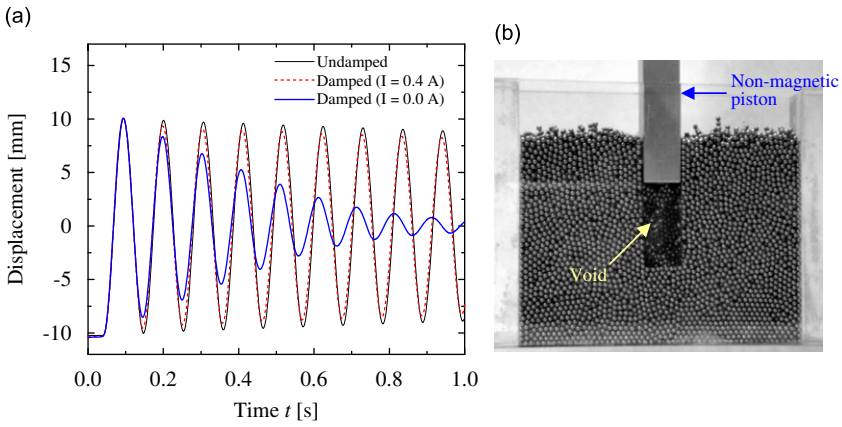


**Fig. 9.** (a) Displacement decay for a non-magnetic piston and (b) the void formed by the piston in a magnetized particle bed.

**Table 2**
Damping capacity for various combinations of particle–particle and piston–particle adhesion.

| State index | Inter-particle adhesion | Piston–particle adhesion | Damping capacity |
|---|---|---|---|
| 1 | Strong | Weak | None |
| 2 | Weak | Weak | Moderate |
| 3 | Weak | Strong | Moderate |
| 4 | Strong | Strong | High |

State 1 considers a configuration in which the particles are strongly adhesive but their adhesion with the piston is very weak. In this state, damping is not produced due to the following explanation. As the piston descends into the particle bed, the particles are packed around it, and when it emerges from the bed during the upstroke, it leaves a void in its place (Fig. 9b). Due to high inter-particle adhesion, the particles are unable to fill the void, thereby preventing the piston from experiencing any damping force during its future oscillations. The system that uses magnetic particles and non-magnetic piston with $I$=0.4 A experiences this state. This system mimics the damping behavior of nanoparticles, which are highly cohesive in their dry form due to strong van der Waals attraction [16].

If the inter-particle adhesion is weak, damping is possible regardless of whether or not the piston is adhesive (see States 2 and 3). State 2 is represented by the un-magnetized passive damping system. In State 3, the piston–particle adhesion is strong, which can be made possible for example, by applying a layer of glue to the piston. In this, the damping capacity can only be significantly greater than in State 2 if the piston–particle adhesion is of a long range nature. Otherwise, a layer of particles will attach to the adhesive piston creating a new boundary that is not adhesive thereby reverting the system to State 2.

In State 4, both inter-particle adhesion and piston–particle adhesion are strong. An example of this state is the magnetized system ($I \neq 0.0$ A) with magnetic particles and magnetic piston. The damping capacity is high and voids are prevented because the particles are always in contact with the piston.

Semi-active control essentially helps a damper change its state with the influence of a magnetic field. For example, a system that uses magnetic piston and magnetic particles can increase its damping capacity by transitioning from State 2 (moderate damping) to State 4 (high damping) by increasing $I$ from 0.0 to 0.4 A. In contrast, a system that uses a non-magnetic piston and magnetic particles can decrease its damping capacity by transitioning from State 2 (moderate damping) to State 1 (no damping) also by increasing $I$ from 0.0 to 0.4 A. Analyzing the transition process provides information regarding the onset, saturation and the range of tunability achievable with semi-active control.

### 4.3. Tunability range

In Fig. 10, the range of damping rates made possible by varying the current $I$ from 0.0 to 0.5 A is presented for the cases with a magnetic or a non-magnetic piston. The experiments were conducted by first measuring the damping with $I$=0.0 A and then incrementally increasing the current from 0.1 to 0.5 A. The magnetic field was turned off in between measurements to allow the particles in the bed to reassemble, and thus to avoid any possible history dependence. The damping rate is represented by a critical decay time ratio given by

$$\Phi = \left(1 - \frac{\tau_d}{\tau_n}\right) \tag{5}$$

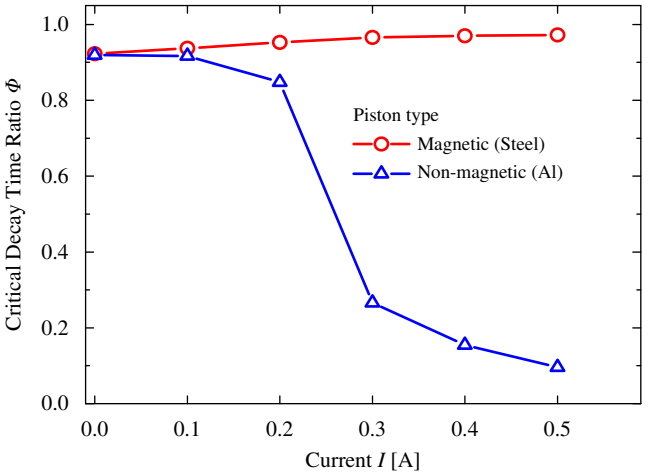


**Fig. 10.** The damping increases with a magnetic piston and decreases with a non-magnetic piston as the magnetic field is strengthened by increasing the current $I$ supplied to the electromagnet.

where $\tau_d$ and $\tau_n$ are defined as the critical decay times required for a damped and undamped system (i.e. passive system without any particles) to reach $1/e$ of the initial energy $E(t_1^1)$, respectively. The parameter $\Phi$ represents damping capacity scaled between 0 and 1 such that the value of $\Phi$=0 signifies no damping and $\Phi$=1 represents maximum damping. Fig. 10 shows that when $I$=0.0 A, the system is in State 2 and both the piston types result in $\Phi$=0.92; i.e. the damping system achieves 92% of the maximum damping. This point is designated as the passive damping offset and it can be adjusted by changing the parameters of the damping system, such as the sizes of the particles, container or piston, the mass of the particles, or the immersion depth of the piston [16]. For a magnetic piston, the onset of tunability is immediate as $\Phi$ increases steadily from 0.92 to 0.98 with each 0.1 A increment in $I$. Although this increase in $\Phi$ appears small, it translates to significant increase in damping rate. For example, when $\Phi$=0.92 ($I$=0.0 A), the displacements decay in 9 cycles and within 1.0 s. By comparison, when $\Phi$=0.98 ($I$=0.4 A), the displacement decay after just 2 cycles and in less than 0.25 s. The displacement decays for the above mentioned cases can be seen in Fig. 6.

For damping with the non-magnetic piston, the onset of tunability is not immediate because $\Phi$ is constant for $I \leq 0.1$ A, which indicates that the magnetic inter-particle adhesion is not sufficient to prevent the particles from flowing. For $0.1\text{ A} < I < 0.2$ A, adhesion become noticeable and a void begins to form under the piston tip, causing $\Phi$ to decrease by 18%. The parameter $\Phi$ decreases nonlinearly as $I$ increases. A critical current value is reached when $0.2\text{ A} < I < 0.3$ A, during which the magnetic inter-particle adhesion becomes dominant, thus preventing any flow of particles, causing the void to become prominent. As a result $\Phi$ drops from 0.82 to 0.25. As $I$ increases further, $\Phi$ tends to zero as the piston continues to oscillate inside the void without any damping resistance. It is possible that the entire range of tunability from $\Phi$=0 to 1, can be achieved by a single piston, if designed to change from non-magnetic to highly magnetic in the presence of a magnetic field.

### 4.4. Demagnetization effect

We have observed that magnetizing the system takes it from one state to another. It is important to study the demagnetization effect to see whether the system can revert back to its original state or not. The demagnetization response is analyzed for experiments with a magnetic and a non-magnetic piston. In both the experiments, the system is magnetized by increasing $I$ from 0.0 to 0.5 A with 0.1 A interval and then demagnetized by decreasing the current to 0.0 A with the same interval. The initial amplitude of the piston is kept constant. In order to capture any history effect caused by the changes in the magnetization levels, the magnetic field was never turned off between tests. Fig. 11a shows that with the magnetic piston, the system transitions from State 2 to State 4 during magnetization and returns to State 2 after demagnetization. A void formation under the piston tip as seen in Fig. 9b does not occur in this system. Since the value of $\Phi$ is same at all value of $I$ during both magnetization and demagnetization, the damping is completely reversible and therefore the system is history independent. This is a desired feature since it implies that the damping represented by the ratio $\Phi$ is a single valued function of current $I$. This behavior is possible as a consequence of the material selected for the particle medium and the piston does not have magnetic hysteresis (Fig. 2b).

In the case of the non-magnetic piston, the system goes from State 2 to State 1 as it is magnetized because a void forms below the piston tip, and as the system is demagnetized, the void becomes filled and the system returns to State 2. However, $\Phi$ is not the same at each value of $I$ during magnetization and demagnetization, which implies that the system with non-magnetic piston exhibits a hysteretic behavior, as seen in Fig. 11b. Since the magnetization of the particles is

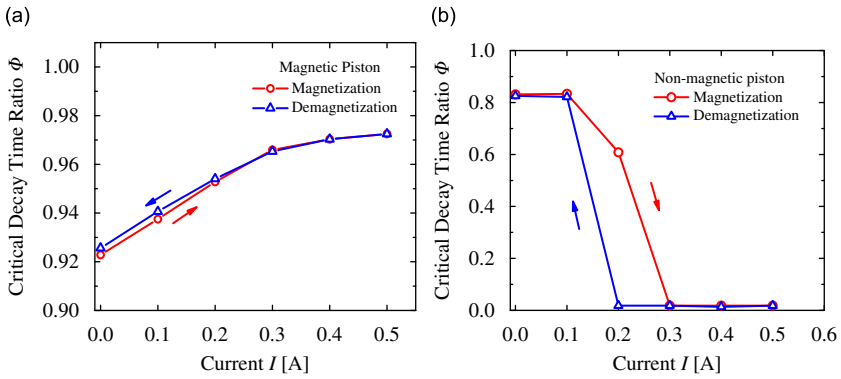


**Fig. 11.** Hysteresis during demagnetization for (a) magnetic and (b) non-magnetic piston.

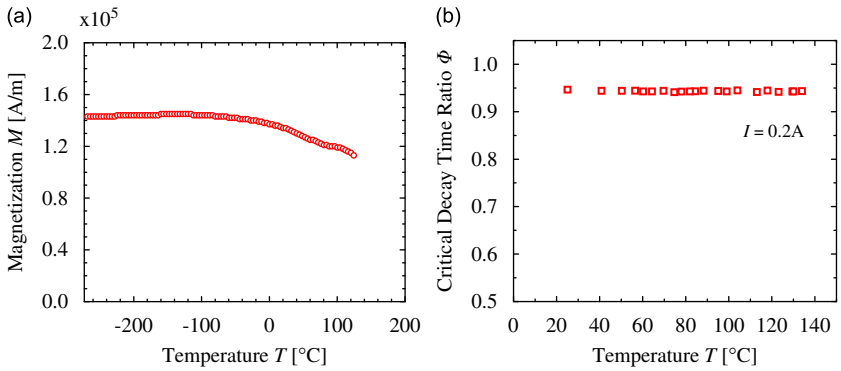


**Fig. 12.** Effect of the temperature on the magnetization $M$ (a) and the damping performance of 1 mm chrome steel particles (b).

hysteresis-free and the piston in non-magnetic, the observed hysteresis is not due to the magnetic properties of the system but is caused by the mechanical process of forming and recovering the void.

### 4.5. Temperature effect

When heated to a sufficiently high temperature, a ferromagnetic material becomes paramagnetic, which causes a significant drop in its magnetization $M$ [14]. This transition temperature is the Curie temperature $T_c$ and can affect the damping rate of a semi-active system. The value of $T_c$ is 770 °C for iron, 385 °C for nickel, and 1130 °C for cobalt [14]. Even below $T_c$, the magnetization can still be temperature dependent. Therefore, the temperature sensitivity of a particle-based semi-active damping system must be examined. Two experiments are performed, each over a wide temperature range. The first examines the change in magnetization of a single particle and the second examines the damping response of the entire particle system.

In the first experiment $M$ is measured for a single 1.2 mm chrome steel particle of mass $m_p$=8.5 mg, for $T$ in the range from $-268$ °C up to 124 °C using a sensitive magnetometer. The magnetic field $H$ is kept constant at 40.8 kA/m and measurements are made at increments of 4 °C. The magnetization appears to be constant for low temperatures ($T<0$ °C) and decreases by 20% as $T$ increases from 0 to 124 °C (Fig. 12a). Therefore, magnetization of the particles is temperature independent when $T<0$ °C.

Sensitivity in damping performance resulting from the variation in $M$ for $T>0$ °C is investigated in the second experiment where a particle bed is used to examine the damping performance. The bed is heated from room temperature at $T$=20–140 °C using a hot plate. The particles are stirred intermittently to ensure uniform heating. A constant magnetic field with $I$=0.2 A is then applied. Twenty damping tests are conducted at various temperatures as the particle bed is cooled back to room temperature. For each test, the temperature of the bed is measured and the damping ratio $\Phi$ calculated. The results are presented in Fig. 12b, which show that the damping performance is constant over a 120 °C temperature range. Even though the magnetization $M$ of an individual particle decreases slightly with increasing temperature, the damping performance of a collection of particles, under a constant magnetic field, is not affected by temperature and also suggests that temperature has a negligible effect on the particle–particle or the particle–piston magnetic interaction. Based on experimental evidence, it can be concluded that semi-active damping using magnetic

particle medium is temperature independent from $-268$ °C to at least 140 °C, as was also observed in the passive damping system [16].

## 5. Conclusions

A semi-active particle-based damping system, which uses a dry magnetic particle bed to absorb and dissipate the energy of a vibrating piston, is designed and investigated. The damping efficiency is tunable by controlling the electric current supplied to generate a magnetic field. For the case in which a magnetic piston is used, the magnetization of both particles and pistons can improve the damping efficiency until the magnetization saturates. If both the particles and pistons are free of magnetic hysteresis, their demagnetization can reverse the damping system to its original un-magnetized status; i.e. the entire system is reversible during the process of magnetization and demagnetization. As a result, the damping rate is predictable, which ensures well-characterized tunability. In contrast, for the case with a non-magnetic piston, the damping system achieves the highest efficiency when particles are not magnetized, and the efficiency decreases with increasing magnetization. Under the tip of the non-magnetic piston, a void forms whose size increases as magnetization increases and reduces the damping force and thus the efficiency.

Within a magnetic field, damping is proved to be independent of temperature over a certain temperature range. Specifically, damping with chrome steel particles is unaffected as the temperature varies between 20 and 140 °C, although the magnetization of the particles decreases by less than 20%. Furthermore, the magnetization of a single chrome steel particle is found unchanged when the temperature spans from $-268$ to 0 °C, which predicts that the damping performance also would not be affected by temperature variation within this range.

It is concluded that for the design of a semi-active particle-based damping system, the particles and the piston must be ferromagnetic to achieve high damping efficiency and free of magnetic hysteresis to obtain a predictable damping rate. For use in high temperature applications, magnetic material must be selected based on their melting point and Curie temperatures.

## Acknowledgment

This research was sponsored by the U.S. Air Force Office of Scientific Research (Grant no. FA9550-05-1-0185/P00003) and supported by the U.S. National Science Foundation IGERT program on Virtual Tribology at Northwestern University. The authors are grateful Profs. Paul Umbanhowar, John Ketterson, Michael Peshkin, Kornel Ehmann and Arthur Schmidt as well as Dr. Oleksandr Chernyashevskyy and Dr. Aaron Greco for expert advice and helpful discussions.

## References

[1] J.B.F. Spencer, S. Nagarajaiah, State of the art of structural control, *Journal of Structural Engineering* 129 (2003) 845–856.
[2] Y.M. Parulekar, G.R. Reddy, Passive response control systems for seismic response reduction: a state-of-the-art review, *International Journal of Structural Stability and Dynamics* 9 (2009) 151–177.
[3] M.D. Symans, M.C. Constantinou, Semi-active control systems for seismic protection of structures: a state-of-the-art review, *Engineering Structures* 21 (1999) 469–487.
[4] M.F. Winthrop, R.G. Cobb, Survey of state-of-the-art vibration isolation research and technology for space applications, San Diego, CA, United States, 2003, pp. 13–26.
[5] T.T. Soong, *Active Structural Control: Theory and Practice*, Wiley, New York, 1990.
[6] T.T. Soong, A.M. Reinhorn, Y.P. Wang, R.C. Lin, Full-scale implementation of active control. I. Design and simulation, *Journal of Structural Engineering New York, NY* 117 (1991) 3516–3536.
[7] J.D. Carlson, B.F. Spencer Jr., Magneto-rheological fluid dampers for semi-active seismic control, *Proceedings of the Third International Conference in Motion and Vibration Control*, 1996, pp. 35–40.
[8] S.J. Dyke, B.F. Spencer, M.K. Sain, J.D. Carlson, Modeling and control of magnetorheological dampers for seismic response reduction, *Smart Materials and Structures* 5 (1996) 565–575.
[9] S.J. Dyke, B.F. Spencer Jr, M.K. Sain, J.D. Carlson, Experimental study of MR dampers for seismic protection, *Smart Materials and Structures* 7 (1998) 693–703.
[10] G. Yang, B.F. Spencer Jr, J.D. Carlson, M.K. Sain, Large-scale MR fluid dampers: modeling and dynamic performance considerations, *Engineering Structures* 24 (2002) 309–323.
[11] A.K. Agnihotri, S.G., Sadler, Magnetic particle damper apparatus, U.S. Patent No. 6260676 B1, 2001.
[12] D.B. Montgomery, *Solenoid Magnet Design; the Magnetic and Mechanical Aspects of Resistive and Superconducting Systems*, Wiley-Interscience, New York, 1969.
[13] J.S. Beetson, *Visualizing Magnetic Fields: Numerical Equation Solvers in Action*, Academic Press, London, 2001 (with CD-ROM).
[14] D. Jiles, *Introduction to Magnetism and Magnetic Materials*, 2nd ed., Chapman and Hall, London, New York, 1998.
[15] X. Fang, J. Tang, Granular damping in forced vibration: qualitative and quantitative analyses, *Journal of Vibration and Acoustics* 128 (2006) 489–500.
[16] B.M. Shah, D. Pillet, X.-M. Bai, L.M. Keer, Q. Jane Wang, R.Q. Snurr, Construction and characterization of a particle-based thrust damping system, *Journal of Sound and Vibration* 326 (2009) 489–502.